

# Joule heating of logs for phytosanitary purposes and timber processing pre-treatment

William J.B. Heffernan\*, Nurzhan Nursultanov, Ryan van Herel, Thomas Smart

University of Canterbury Electric Power Engineering Centre, Christchurch, 8001, New Zealand

\*Corresponding author

DOI: 10.5185/amlett.2018.2133

www.vbripress.com/aml

## Abstract

Joule heating has recently been investigated as a potential alternative to chemical fumigation for phytosanitary treatment of *Pinus radiata* logs exported from New Zealand. The research was driven by concern regarding the effects of methyl bromide release to atmosphere, following fumigation, as highlighted by the Montreal Protocol. The work has involved creating 1 dimensional and 3 dimensional computer models of the Joule heating process in *P. radiata*, building a laboratory-scale log test rig with suitable instrumentation and control systems, heating approximately 60 *P. radiata* logs and using the measured data to refine and validate the models. While engaged in this work it became clear that the process could also potentially be applied to heat veneer peeler logs. This paper describes the application of the 1 dimensional model and laboratory-scale test rig to a typical *P. radiata* export log and to a *Eucalyptus nitens* log prepared for veneer peeling. The results demonstrate that, despite the heterogeneities of the timber, the technique is capable of achieving the required temperature profiles for both applications and that the model is a sufficiently good representation of the process to provide a viable control method. Copyright © 2018 VBRI Press.

**Keywords:** Ohmic heating, joule heating, phytosanitary treatment, peeler log heating, CFD modelling.

## Introduction

In 2007 the suggestion was made by Grant Knight, a biosecurity expert with the NZ Ministry of Agriculture and Forestry (now Ministry of Primary Industries) that Joule heating might be worth investigating as a heat-treatment alternative to the methyl bromide fumigation process currently employed in NZ for phytosanitary treatment of a significant proportion of export logs. (The main purpose of such treatments is the destruction of all life stages of certain species of bark and ambrosia beetles [1]). A replacement technology was needed as compliance with the Montreal Protocol was leading to tightening restrictions on the release of methyl bromide to atmosphere, due to its ozone depleting properties. Although not yet formally accepted as a qualifying heat-treatment method, if Joule heating of green (unseasoned) logs could achieve the goals of International Phytosanitary Standard ISPM-15, namely exceeding 56°C for at least 30 minutes [2], it could be shown to be technically viable.

Joule heating has previously been considered as a pre-peel heat treatment for plywood veneer logs, with reporting of an early experimental approach [3, 4] and later computational modelling [5]. However, in the earlier papers [3, 4], although they noted the formation of hot and cold spots in the heterogeneous timber, the authors had no model of the electro-thermal process from which to gain sufficient insight into its causes or mitigation. Furthermore they did not have a well-

controlled electrical excitation system and were thus unable to adequately regulate the specific current and power density in the timber. The later work [5] was entirely based on computational modelling, with no experimental validation, and unfortunately did not adequately consider the very significant temperature coefficients of electrical conductivity. (The main purpose of this heat treatment is the softening of lignins [5], leading to easier veneer cutting with higher quality results).

The failure of these earlier works to combine modelling, for in-depth understanding of the process, and experimentation, for model validation, appears to have led to the abandonment of the idea.

Our initial approach was to characterize the electrical and thermal properties of green *P. radiata* as functions of wood type (sap/heart), temperature, grain orientation, moisture content and basic density, using small timber samples [6, 7]. The most significant finding [6] is that, at the relatively high sapwood moisture contents (MC) typical of green logs (well above fibre saturation), the electrical conductivity (EC) is very strongly dependent on temperature and virtually independent on MC, which agrees well with the substantial body of published work by Stamm [8, 9, 10], who was primarily concerned with the effect of MC, and not temperature, on EC, in his work on developing electrical moisture meters (for use on relatively dry timber).

Using the characterized data, 3-dimensional (3-D) electro-thermal models were created in ANSYS-CFX computational fluid dynamics (CFD) software [7]. A simplified 1-dimensional (1-D) model was also created in MATLAB. The 3-D and 1-D models were compared for typical log dimensions, with typical heart and sapwood proportions, and found to be sufficiently close to allow the 1-D model to be used to control the operation of the 100kW laboratory-scale heating system previously built [11]. (This is advantageous as the 1-D model computes in seconds, whereas the 3-D models take several hours to run).

This system was used to heat about 60 *P. radiata* logs with a length of 3.3m and volumes between about 0.25 and 0.45m<sup>3</sup>. Operating under constant power control, the model calculates the inter-related distributions of power dissipation and temperature rise within the log, along with the expected total electrical resistance for direct comparison with the resistance of the real log measured in real-time. It also calculates the required energy to heat the log from a measured initial equilibrium temperature to a desired average sapwood temperature.

Since real logs are heterogeneous, with features such as knots, bark inclusions and resin pockets, a regime of 100kW constant power “excitation” periods followed by temperature equilibrating “relaxation” periods [11] was developed, capable of ensuring all measured “cold” spots in the initial 32 test logs exceeded the ISPM-15 minimum of 56°C [1]. There are many aspects involved in this implementation of the Joule heating process that cannot be covered in a single paper. These form the subject of a number of publications currently in process and include:

- Design and implementation of segmented electrodes to achieve good electrical contact to log ends, along with real-time current measurement for verification of model-predicted current density distribution.
- Modelling and experimental verification of the effects of knots and other heterogeneities in a range of pruned and unpruned logs with various branching habits and how this affects the choice of effective excitation and relaxation schemes to achieve sufficiently uniform heating, verified by statistically significant numbers of post-treatment invasive temperature measurements on a significant number of treated logs.
- Computed tomography imaging of logs to find heterogeneities in real-time and infer their effects on heating uniformity.
- Electro-thermal characterization of other timber species, including *Pseudotsuga menziesii*, *Sequoia sempervirens* and *Eucalyptus nitens*, which have two or three distinct wood zones with different electrical and thermal properties.
- Production-scale implementation covering log-handling logistics, economics and electricity demand levelling.

This paper seeks to give an overview of the critical aspects of the 1-D modelling and laboratory-scale

experimental implementation as applied to a single, typical *P. radiata* log, for phytosanitary purposes, and a single *E. nitens* log, for veneer peeling purposes.

## Computational and experimental methods

### Computational modelling

Fig. 1 shows the 1-D model cross section of a log containing distinct heartwood (HW) and sapwood (SW) regions.

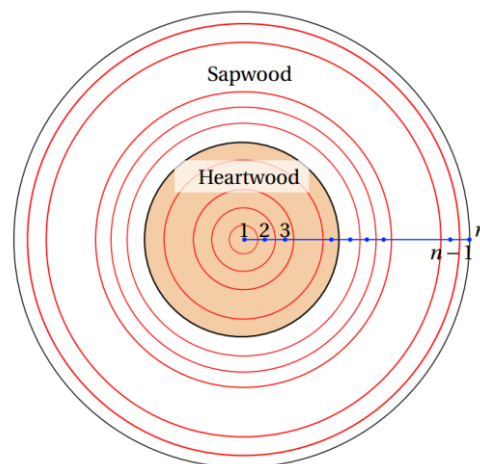


Fig. 1. Division of typical log into 1-D radial control volumes.

We start by considering a set of control volumes from 1 to  $n$  ( $n$  is typically in the region of 500) in the HW and SW regions. These control volumes are essentially nodes on the log’s radius from pith to bark, which when rotated through 360° form thin cylinders running the length of the log. (Of course a real log is more like a truncated cone, with a smaller number of growth rings at the small end than the large end, which forces some radial current flow [6, 7]. However the practical effects of this are relatively minor [7]).

When populated with the required data concerning the properties of the timber species’ HW and SW, the log dimensions and mass, the initial log temperature, the surrounding air temperature and the target temperature, as well as the excitation power, the model calculates the required total energy and the expected electrical resistance of the log during each excitation period. The model achieves this by iteratively solving the heat conservation equation:

$$\frac{\partial \rho_g c_p T}{\partial t} = \nabla \cdot (k \nabla T) + \sigma E^2 \quad (1)$$

where  $\rho_g$  is the green density of the timber’s HW or SW,  $C_p$  is the specific heat capacity,  $k$  is the thermal conductivity,  $\sigma$  is the EC,  $T$  is the temperature and  $E$  is the electric field strength along the log.

The model also assumes conservation of electric charge:

$$\nabla \cdot (J) = \nabla \cdot (\sigma E) = 0 \quad (2)$$

where  $J$  is the current density in the log.

For *P. radiata*, the longitudinal SW EC, as a function of temperature, is given as [6]:

$$\sigma_{LSW} = \exp \left[ -2.60 + 0.017(T - 55) - 0.073 \frac{(T-55)^2}{1000} \right] \quad (3)$$

With the HW EC being so close to zero as to be negligible.

For *E. nitens*, the longitudinal SW EC, as a function of temperature, is given as:

$$\sigma_{LSW} = \exp \left[ -1.855 + 0.017(T - 55) - 0.08 \frac{(T-55)^2}{1000} \right] \quad (4)$$

while for HW EC is given as:

$$\sigma_{LSW} = \exp \left[ -2.83 + 0.018(T - 55) - 0.074 \frac{(T-55)^2}{1000} \right] \quad (5)$$

Note therefore that the HW of *E. nitens* is nearly as conductive as the SW of *P. radiata*, while its SW is significantly more conductive.

Starting at the initial log temperature (usually assumed to be equilibrated throughout the timber), the log's resistance, R, is calculated and the appropriate value of voltage across the log,  $V_{hv}$ , is chosen to give the correct excitation power, P:

$$V_{hv} = \sqrt{P \cdot R} \quad (6)$$

As each successive iteration is performed each control volume heats up and takes the appropriate new value for EC, the resulting conductances of the electrically parallel control volumes being summed to give the overall log conductance, S, the reciprocal of which is the log's electrical resistance, R, at that time-step. In this way, the profile of R versus time is built up over the successive excitations and relaxations.

The model estimates the total energy,  $W_T$ , injected to reach the required log temperature, calculated as:

$$W_T = m C_p (T_f - T_i) \quad (7)$$

where  $T_i$  and  $T_f$  are the initial and target temperatures, respectively, and  $m$  and  $C_p$  are the mass and heat capacity of the log region where Joule heating occurs, respectively. For *P. radiata*, Joule heating occurs almost entirely in the SW, while for *E. nitens* Joule heating occurs in both the SW and HW. Thus, the total energy injected into the *E. nitens* log is estimated as:

$$W_T = (m_{SW} C_{p_{SW}} + m_{HW} C_{p_{HW}}) (T_f - T_i) \quad (8)$$

Generally the model makes some simplifications in which the green density of the SW and HW are assumed to have typical specific values, with the MCs adjusted to match the HW and SW volumes with the experimentally measured mass for a given log.

### Experimental procedure

The laboratory-scale experimental rig is designed to heat logs up to 3.3m in length and 0.5m in large end diameter (LED) and consists of several parts:

- Thermally insulated chamber with 20kW heating system – allows surrounding air temperature to be

controlled. (An optional 18kW steam humidification system has also been implemented).

- Electrically insulating log supports with built in load-cells for real-time mass measurement.
- Pneumatic-ram driven segmented electrode at each log end with 30 equal-area segments, each with independent optically isolated current measurement, and open-cell foam conformal pad with pneumatically driven electrically conductive gel injection system, to give low contact resistance to timber.
- 0 to 400V variable low voltage (LV), alternating current (AC) single phase power supply, with voltage, current, power and totalized energy instrumentation and control system with constant power control, bounded by maximum voltage (400V), maximum current (500A) and maximum power (120kW) constraints.
- High voltage (HV) step-up transformer arrangement consisting of two 150kVA 230V to 11.5kV single phase transformers with series connected LV primaries and selectable (by pneumatically operated switch) series or parallel HV secondary windings, which are used to match constant excitation power to the variable log resistance.
- Zigbee wireless HV-side current and voltage sensors, PT100 chamber temperature sensors and capacitive element chamber humidity sensors.
- LabVIEW-based data acquisition system.
- Independent LV-side voltage, current and power analyser and logger (Fluke 435).

Fig. 2 shows the matching of any log resistance between 250Ω and 4kΩ to 100kW constant excitation power, P. For resistances above 1kΩ the secondary windings must be in series (Connection B), with a parallel connection below this resistance (Conn A). (NB. Connection C is neither needed nor implemented). Power deliverable to log resistances above 4kΩ is voltage limited to 20kV, while to those below 250Ω it is current limited to 20A. In practice the load-matching range is adequate for heating real logs within the dimensional constraints of the rig.

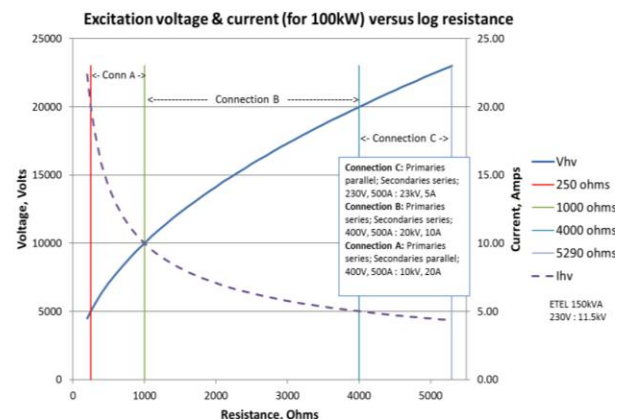


Fig. 2. HV-side voltage and current for 100kW, versus resistance.

For any log resistance, along the x-axis, the log voltage is given by the solid  $V_{hv}$  line (left hand y-axis) and the log total current is given by the dashed  $I_{hv}$  line (right hand y-axis). Since lethal voltage is present across the log, safety best practice is followed, including:

- Grounding the centre-point of the HV windings, when series connected, giving a maximum system voltage of 10kV relative to ground.
- Instituting minimum approach distance to rig when livened.
- Attaching earth wands to HV bushings when rig is unlivened.

### Results and discussion

**Table 1** gives the parameters required by the 1-D model for both the *P. radiata* phytosanitary treatment log and the veneer peeling *E. nitens* log.

**Table 1.** Log and treatment parameters.

Parameter	<i>P. radiata</i>	<i>E. nitens</i>
Log LED, m	0.436	0.320
Log SED, m	0.399	0.316
HW SED, m	0.210	0.240
HW LED, m	0.190	0.210
Log length, m	3.2	3.3
Log mass, kg	437	228
Initial temperature, °C	26	20.5
HW Basic Density, $kgm^{-3}$	400	427
HW MC, $kgkg^{-1}$	0.5	1.0
SW Basic Density, $kgm^{-3}$	450	405
Log volume, $m^3$	0.44	0.26
SW volume, $m^3$	0.34	0.13
HW volume, $m^3$	0.10	0.13
SW mass, kg	379	116
SW MC, $kgkg^{-1}$	1.5	1.2
Chamber temperature, °C	60	60
Number of excitations	3	6
Relaxation duration, minutes	10	10, 20
Number of time-steps	500	500
Number of control volumes	500	500
Target temperature, °C	75	75
Total energy required, kWh	15.7	9.6
Energy per $1m^3$ of SW, kWh	47	57
Energy per $1m^3$ of log, kWh	36	37

The first set of parameters (normal type) are physical measurements which are made and entered into a purpose-built GUI. The second set (underlined) are estimated values based on empirical data (and can be verified post-treatment using samples from the actual log tested if required). From these, the volumes and masses of HW and SW and the SW MC (italics) are calculated and used in the model. The next parameter set (underlined) are environmental and temporal parameters that are chosen for the model and must be adhered to in the experiment. The next set (bold type) are modelling parameters and the termination condition, resulting in the calculated total energy requirement produced by the model (italics).

**Fig. 3** shows the model calculated and experimental log resistance over the chosen excitation and relaxation regimes for both test logs.

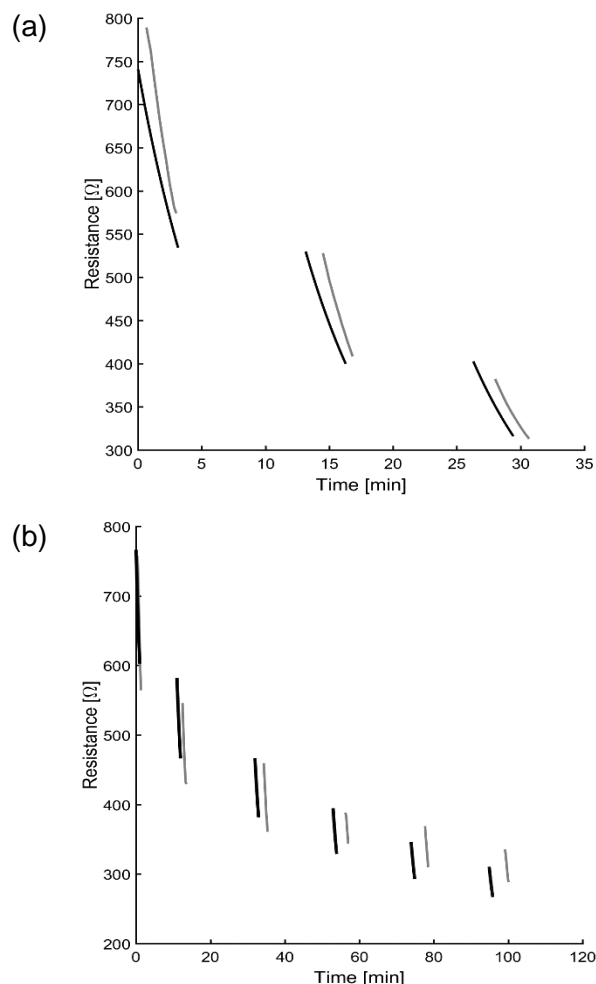


**Fig. 3.** Resistance versus time for logs (a) *P. radiata*; (b) *E. nitens*. Black lines are modelled values, grey are experimental.

Note that a three excitation regime is chosen for the *P. radiata* log, with the total energy split equally between the excitations, and relatively short ten minute relaxation periods between excitations. With the *E. nitens* log a six excitation regime is chosen with longer relaxation periods. This is for two reasons: Firstly the heating has been found to be generally less even in *E. nitens*, requiring more time for hot and cold spots to equilibrate; secondly the aim is to penetrate the heat deeper into the log for the peeling application, as all parts of the log need to be heated [4, 5], whereas in the phytosanitary application the penetration depth can be more limited [1]. Note further that, even when cold, both logs had a resistance less than  $1k\Omega$ , such that only the parallel HV winding configuration was needed. Additionally there was some delay in starting the experimental excitations, but despite this the agreement between modelled and measured resistance is generally better than 10% of the predicted value. The resistance reduces by a factor of about 2.5 for the *P. radiata* log and 3 for the *E. nitens* log, respectively.

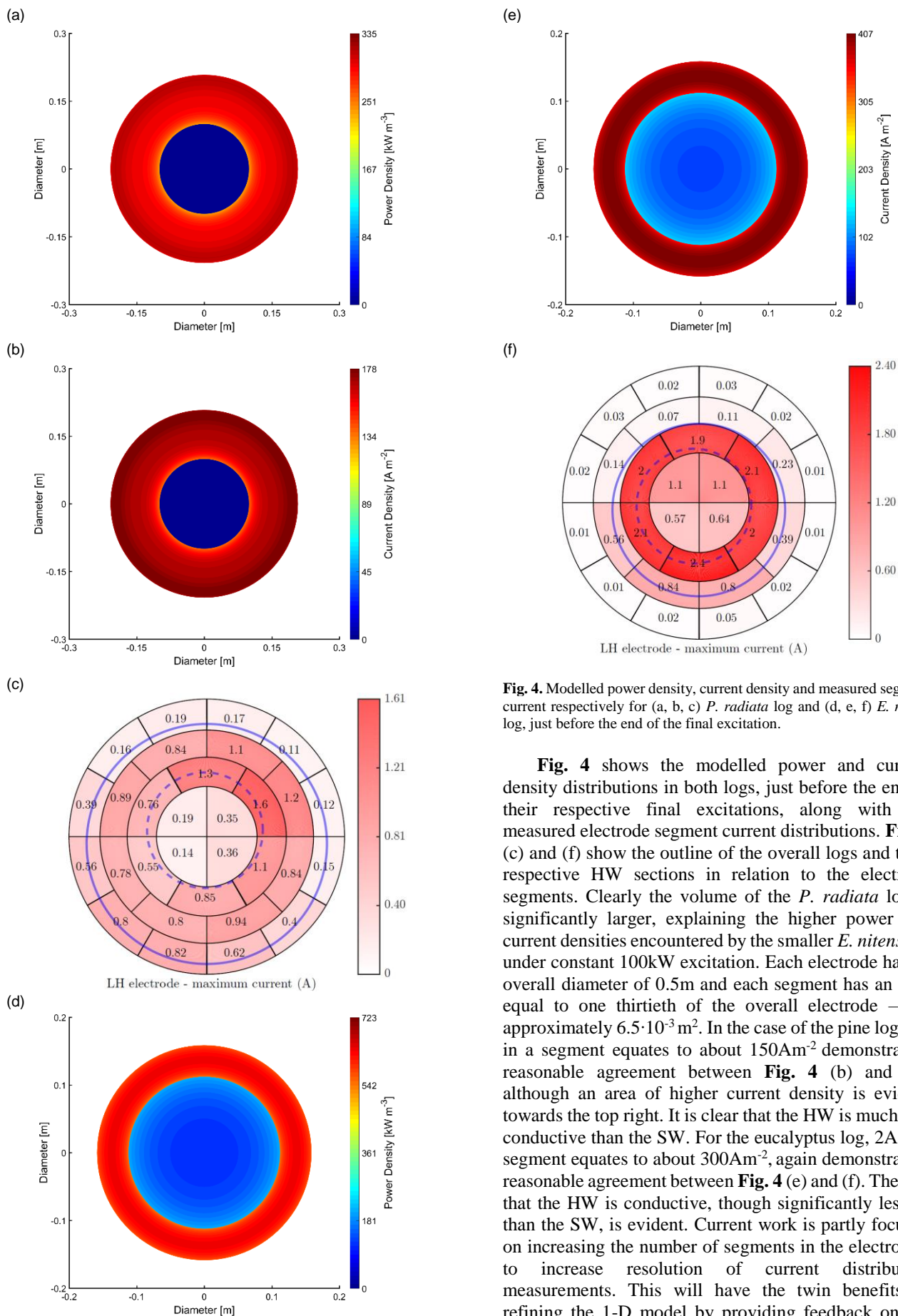
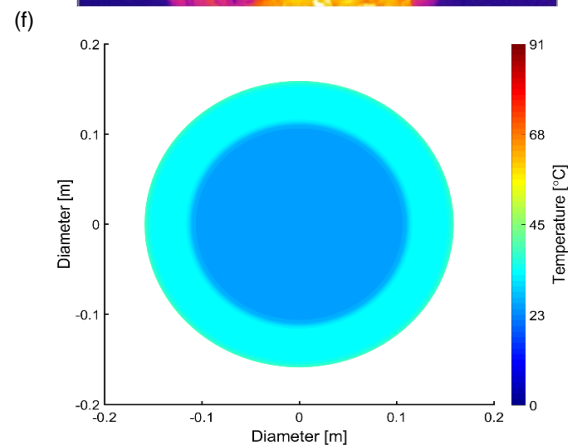
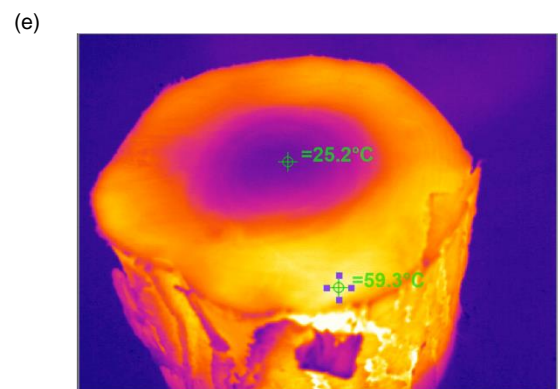
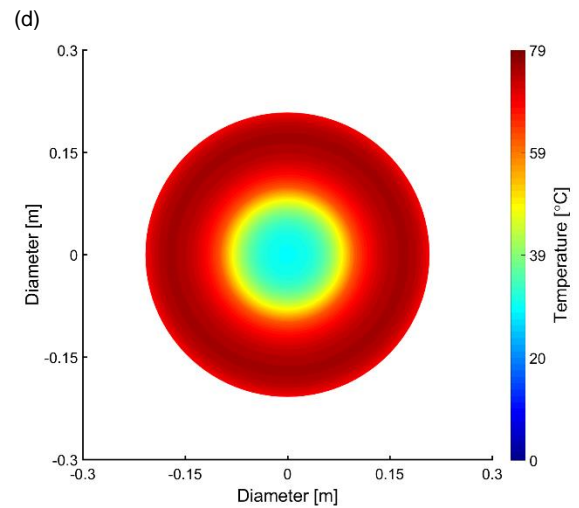
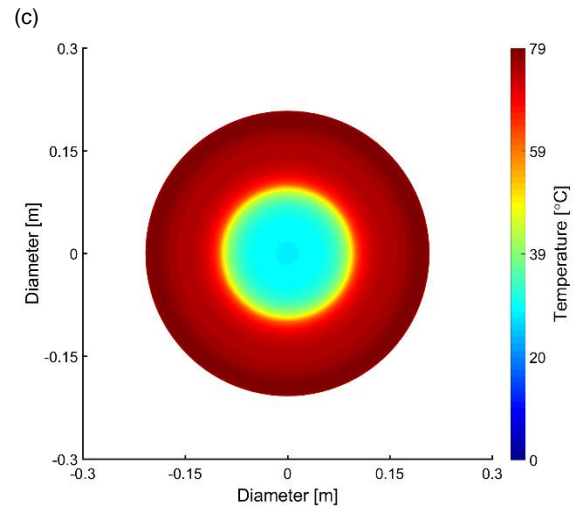
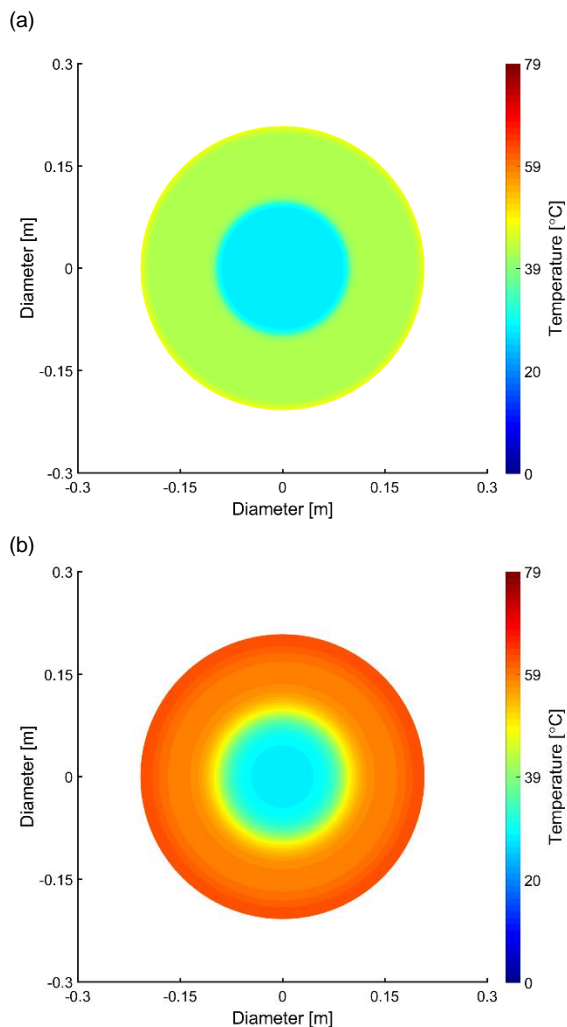


**Fig. 4.** Modelled power density, current density and measured segment current respectively for (a, b, c) *P. radiata* log and (d, e, f) *E. nitens* log, just before the end of the final excitation.

**Fig. 4** shows the modelled power and current density distributions in both logs, just before the end of their respective final excitations, along with the measured electrode segment current distributions. **Fig. 4** (c) and (f) show the outline of the overall logs and their respective HW sections in relation to the electrode segments. Clearly the volume of the *P. radiata* log is significantly larger, explaining the higher power and current densities encountered by the smaller *E. nitens* log under constant 100kW excitation. Each electrode has an overall diameter of 0.5m and each segment has an area equal to one thirtieth of the overall electrode – i.e. approximately  $6.5 \cdot 10^{-3} \text{ m}^2$ . In the case of the pine log, 1A in a segment equates to about  $150 \text{ Am}^{-2}$  demonstrating reasonable agreement between **Fig. 4** (b) and (c), although an area of higher current density is evident towards the top right. It is clear that the HW is much less conductive than the SW. For the eucalyptus log, 2A in a segment equates to about  $300 \text{ Am}^{-2}$ , again demonstrating reasonable agreement between **Fig. 4** (e) and (f). The fact that the HW is conductive, though significantly less so than the SW, is evident. Current work is partly focused on increasing the number of segments in the electrodes, to increase resolution of current distribution measurements. This will have the twin benefits of refining the 1-D model by providing feedback on the

resistance and temperature of individual control volumes, as well as providing clear dimensional information on the SW/HW boundary, which will obviate the need for optical log diameter measurements prior to treatment.

**Fig. 5** demonstrates the modelled heating profile for both logs at different stages in the excitation and relaxation process. **Fig. 5** (a) & (f) clearly show the division between HW and SW, with the majority of temperature rise occurring in the more conductive SW during the first excitation. **Fig. 5** (b) & (g) show that by the beginning of the final excitation, heat has started to spread into the HW, especially in the eucalyptus case where some energy has been introduced directly by Joule heating in the HW and also more time has elapsed for heat diffusion from the SW. **Fig. 5** (c) & (h) show the maximum temperatures that are reached in the SW – it is important to ensure that these do not exceed boiling point, which is a little over 100°C for sap in wood at atmospheric pressure, or else checking or other damage will occur in the timber. **Fig. 5** (d) & (i) show how the heat has diffused 30 minutes after the last excitation, indicating in (d) that the outer 100mm annulus is well above 60°C and in (i) that all the wood is between 45°C and 80°C.



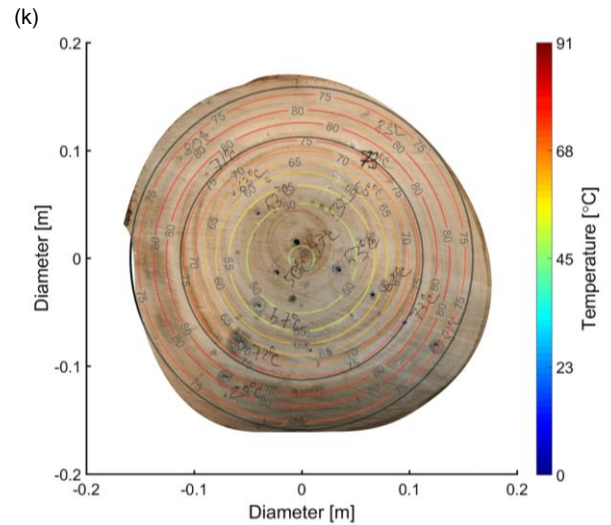
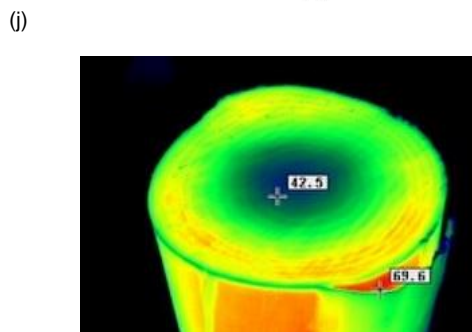
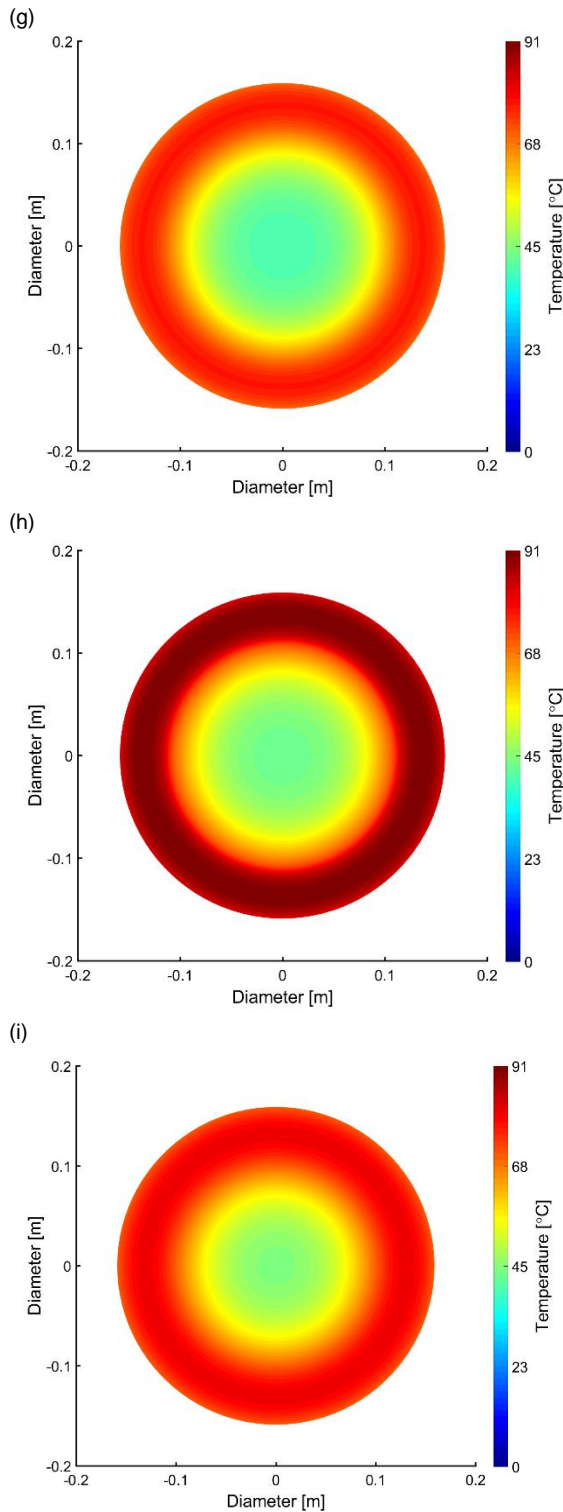


**Fig. 5.** Modelled heating profiles at the end of the first excitation, beginning of the final excitation, end of the final excitation and 30 minutes after the final excitation for *P. radiata* log (a, b, c, d) and *E. nitens* log (f, g, h, i), respectively; thermal images of sections cut 30 minutes after the final excitation from the *P. radiata* log (e) and *E. nitens* log (j) respectively. In (k), isothermal contours from (i) are overlaid on the same cross-section imaged in (j), in which spot temperatures, in holes drilled 50mm below the surface, have been measured by PT100 sensor and marked in pen as shown. The black rings show the modelled HW/SW boundary and overall log diameter.

Thermal images (e) & (j) (taken with Guide EasIR™-9 infrared camera) for *P. radiata* and *E. nitens*, respectively, have been given to show qualitative agreement with the model results. However, the procedure involves sawing a section from the log in the heated chamber and removing it to the surrounding ambient air for imaging, by which time its surface has cooled significantly. This is because the chamber temperature in the modelled experiments is 60°C, which is beyond the operating environment of the imager – if the imager is briefly taken from a 20°C ambient into the heated chamber, water vapour condenses on the cold silicon lens and distorts the measured temperatures. To show true timber temperature there is no alternative to drilling holes and measuring in the resulting thermowell with PT100 instruments. **Fig. 5** (k) shows a set of such spot temperature measurements (made with a calibrated Center 370 PT100 RTD Thermometer, with total measurement uncertainty of about +/-0.5°C, in the same section used for thermal image (j)) with contemporaneous contours from the model (i) for direct comparison. There is very close agreement between the model (i) and spot measurements (k), indicating that the model is accurate and reliable.

**Fig. 6** shows the energy generation and transfer in both log cases.

**Fig. 6** (a) shows that the Joule heating energy in the *P. radiata* log’s HW is negligible, as expected. It also shows that over the 30 minutes of Joule heating excitations and relaxations and 30 minutes of heat equilibration after the last excitation, about 1.5kWh of energy diffuses from the SW to the HW. Also, during the excitations and relaxations the log surface absorbs about

0.4kWh from the chamber air, which it then returns during the 30 minute post-excitation equilibration period. On the other hand, **Fig. 6 (b)** shows that, although the eucalyptus HW is less electrically conductive than the SW it nevertheless generates a significant amount of Joule heat (equal to just over 20% of the log's total). During the whole process a little over 3kWh of energy diffuses from the SW to the HW, while the log first absorbs about 0.4kWh from the chamber air before finally returning about 1kWh to the air by the end of the process.

It can therefore be noted that in both cases there is a net increase in chamber air energy. Hence, if well enough insulated and if having sufficient air capacity, the elevated chamber temperature can be at least partly sustained by waste heat from the logs.

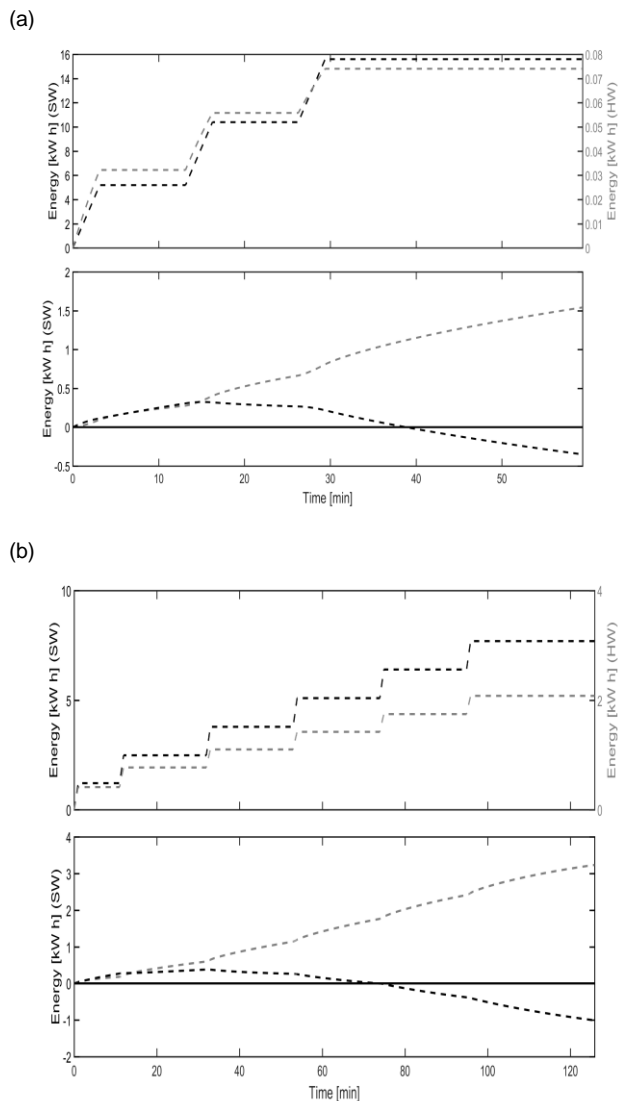


**Fig. 6.** Modelled Joule heating (JH) energy introduced directly into SW and HW, along with energy transfer between SW and HW and between chamber air and log surface for (a) *P. radiata* and (b) *E. nitens*. In each case the top graph shows JH energy generated in SW (black dashed line, left hand y axis) and HW (grey dashed line, right hand y axis). In each case the bottom plot shows energy diffusion from SW into HW (grey dashed line) and convection from chamber air to log surface (black dashed line).

## Conclusion

The reported work shows that Joule heating can be adapted to successfully heat both softwood and hardwood logs to temperatures in the region of 60 to 70°C or so. Such heating requires in the order of 40kWh of energy per cubic metre of timber and can be sufficient both to eliminate pest insects (and other organisms) and to soften timber for veneer peeling and slicing. The heterogeneous nature of timber does not generally allow a single fast burst of energy to be introduced (except perhaps in the special case of pruned logs where all major non-uniformities are contained in a non-conducting heartwood defect core, such as can be achieved with *P. radiata*). Instead the energy must be introduced in multiple excitations, with suitable heat-spreading relaxation periods. Phytosanitary applications, where the pest species of concern are known to be in the outer sapwood can be satisfied within 30 to 60 minutes of starting first excitation. It is generally harder and slower to get heat into the centre of the log, with peeling temperatures for logs with diameters of 300 to 450mm able to be achieved in about two hours, still representing a major time saving over steam and hot-water bath heating.

A production machine can be envisaged in which multiple logs are treated in a chamber, with several logs being excited by several electrode pairs while many others are relaxing. In this way the total electrical load can be controlled at a roughly constant power, achieving low electricity unit cost. The single electrode pair, laboratory-scale, 100kW machine takes just over 9 minutes of excitation time (Fig. 3) to treat the 0.44m<sup>3</sup> *P. radiata* log. Therefore, after the initial 30 to 60 minute complete excitation, relaxation and equilibration cycle, a 1MW modular machine could expel one treated log of similar volume each minute, with additional modules added to achieve any desired throughput.

The value of the technique for phytosanitary applications depends on the desire to reduce the use of fumigants and to be able to adapt treatment regimes rapidly to changing pest threats. The value of the technique to veneer peeling depends on the availability of space for storing unprocessed logs, the cost of the time-lag between log delivery and lathe start-up, the availability of wood-waste for hot-water heating versus alternative potential uses (e.g. biofuel or chemical feedstock) and the cost of electricity.

Based on this work we believe Joule heating's applicability to peeler log heating is worthy of being reconsidered.

## Acknowledgements

This work was funded in part by NZ organizations Stakeholders in Methyl Bromide Reduction (STIMBR) and Ministry of Business, Innovation & Employment (MBIE). The authors would like to also thank Steve Pawson of Scion Research, lead entomologist on the project, as well as David Healy, Paul Agger, Edsel Villa, Nigel Pink, Leigh Richardson and Graham Mitchell, of University of Canterbury, for their technical support.

**Author's contributions**

Conceived the plan: WJH, NN, RvH; Performed the experiments: WJH, NN, RvH, TS; Data acquisition: WJH, RvH, TS; Data analysis: NN, RvH; Wrote the paper: WJH, NN (WJH, NN, RvH, TS are the initials of authors). Authors have no competing financial interests.

**References**

1. Pawson, S.M.; Bader, M.K.F; Brockerhoff, E.G.; Heffernan, W.J.B.; Kerr, J.L.; O'Connor, B. Quantifying the thermal tolerance of wood borers and bark beetles for the development of Joule heating as a novel phytosanitary treatment of pine logs. Under review by *Journal of Pest Science*, **2018**, Submission ID: PEST-D-18-00151
2. IPPC. International standards for phytosanitary measures (ISPM 15), **2016**.  
[https://www.ippc.int/static/media/files/publication/en/2016/06/ISPM\\_15\\_2013\\_En\\_2016-06-07.pdf](https://www.ippc.int/static/media/files/publication/en/2016/06/ISPM_15_2013_En_2016-06-07.pdf). Accessed: 08.05.2018
3. Fleischer, H. O.; Downs, L. E. Heating veneer logs electrically. Technical report No.1958, United States Department of Agriculture, Forest Service, Forest Products Laboratory, **1953**.
4. Lutz, J. F. Heating veneer bolts to improve quality of Douglas-fir plywood. Technical report No.2182, United States Department of Agriculture, Forest Service, Forest Products Laboratory, **1960**.
5. Perré, P. Electrical heating of green logs using Joule's effect: A comprehensive computational model used to find a suitable electrode design. *Wood Science and Technology*, **2004**, 38(6):429–449.
6. Nursultanov, N.; Altaner, C.; Heffernan, W. J. B. Effect of temperature on electrical conductivity of green sapwood of *Pinus radiata* (radiata pine). *Wood Science and Technology*, **2017**, 51(4):795–809.  
**DOI:** [10.1007/s00226-017-0917-6](https://doi.org/10.1007/s00226-017-0917-6)
7. Nursultanov, N. Joule heating of green *Pinus radiata* logs for phytosanitary purposes: An in-depth investigation by experimentation and computational modelling. PhD Thesis, University of Canterbury, New Zealand, **2018**.
8. Stamm, A. J. The electrical resistance of wood as a measure of its moisture content. *Industrial & Engineering Chemistry*, **1927**, 19(9):1021–1025
9. Stamm, A. J. The fiber-saturation point of wood as obtained from electrical conductivity measurements. *Industrial & Engineering Chemistry Analytical Edition*, **1929**, 1(2):94–97
10. Stamm, A. J. Wood and cellulose science. Ronald Press Co., New York: USA, **1964**.
11. Heffernan, W.J.B. Practical application of Joule heating to the sterilization of plantation grown *Pinus radiata* logs. Electricity Engineers' Association Conference, New Zealand, **2013**.